The Astrophysical Journal Supplement Series, 242:4 (15pp), 2019 May https://doi.org/10.3847/1538-4365/ab16f4

Two New Catalogs of Blazar Candidates in the *WISE* Infrared Sky

Raffaele D'Abrusco[1], Nuria Álvarez Crespo[2,3], Francesco Massaro[2,4,5], Riccardo Campana[6], Vahram Chavushyan[7], Marco Landoni[8], Fabio La Franca[9], Nicola Masetti[6,10], Dan Milisavljevic[11], Alessandro Paggi[2,4,5], Federica Ricci[12], and Howard A. Smith[1]

[1] Center for Astrophysics|Harvard & Smithsonian, 60 Garden Street, Cambridge, MA 20138, USA; rdabrusc@cfa.harvard.edu
[2] Dipartimento di Fisica, Università degli Studi di Torino, via Pietro Giuria 1, I-10125 Torino, Italy
[3] European Space Agency (ESA), European Space Astronomy Centre (ESAC), E-28691 Villanueva de la Cañada, Madrid, Spain
[4] Istituto Nazionale di Fisica Nucleare, Sezione di Torino, via Pietro Giuria 1, I-10125 Torino, Italy
[5] INAF—Osservatorio Astrofisico di Torino, via Osservatorio 20, I-10025 Pino Torinese, Italy
[6] INAF—Osservatorio di Astrofisica e Scienza dello Spazio, via Gobetti 93/3, I-40129, Bologna, Italy
[7] Instituto Nacional de Astrofísica, Óptica y Electrónica, Apartado Postal 51 y 216, 72000 Puebla, México
[8] INAF—Istituto Nazionale di Astrofisica, via Emilio Bianchi 46, I-23807 Merate (LC), Italy
[9] Dipartimento di Matematica e Fisica, Università Roma Tre, via della Vasca Navale 84, I-00146, Roma, Italy
[10] Departamento de Ciencias Físicas, Universidad Andrés Bello, Fernández Concha 700, Las Condes, Santiago, Chile
[11] Department of Physics and Astronomy, Purdue University, 525 Northwestern Avenue, West Lafayette, IN 47907, USA
[12] Instituto de Astrofísica and Centro de Astroingeniería, Facultad de Física, Pontificia Universidad Católica de Chile, Casilla 306, Santiago 22, Chile
Received 2018 December 17; revised 2019 February 18; accepted 2019 March 26; published 2019 May 8

Abstract

We present two catalogs of radio-loud candidate blazars whose *Wide-Field Infrared Survey Explorer* (*WISE*) mid-infrared colors are selected to be consistent with the colors of confirmed γ-ray-emitting blazars. The first catalog is the improved and expanded release of the *WISE* Blazar-like Radio-Loud Sources (WIBRaLS) catalog presented by D'Abrusco et al. It includes sources detected in all four *WISE* filters, spatially cross-matched with radio sources in one of three radio surveys and radio-loud based on their q_{22} spectral parameter. WIBRaLS2 includes 9541 sources classified as BL Lacs, flat-spectrum radio quasars, or mixed candidates based on their *WISE* colors. The second catalog, called KDEBLLACS, based on a new selection technique, contains 5579 candidate BL Lacs extracted from the population of *WISE* sources detected in the first three *WISE* passbands ([3.4], [4.6], and [12]) only, whose mid-infrared colors are similar to those of confirmed, γ-ray BL Lacs. Members of KDBLLACS are also required to have a radio counterpart and be radio-loud based on the parameter q_{12}, defined similarly to the q_{22} used for the WIBRaLS2. We describe the properties of these catalogs and compare them with the largest samples of confirmed and candidate blazars in the literature. We cross-match the two new catalogs with the most recent catalogs of γ-ray sources detected by the *Fermi* Large Area Telescope. Since spectroscopic observations of candidate blazars from the first WIBRaLS catalog within the uncertainty regions of γ-ray unassociated sources confirmed that $\sim$90% of these candidates are blazars, we anticipate that these new catalogs will again play an important role in the identification of the γ-ray sky.

Key words: BL Lacertae objects: general – catalogs – galaxies: active – radiation mechanisms: non-thermal

Supporting material: FITS files

1. Introduction

Blazars represent one of the most extreme classes of active galactic nuclei (AGNs). These radio-loud sources are characterized by flat radio spectra even at low radio frequencies (i.e., below $\sim$1 GHz; Massaro et al. 2013a, 2013c; Nori et al. 2014; Giroletti et al. 2016), superluminal motions (see, e.g., Vermeulen & Cohen 1994; Lister & Homan 2005; Lister et al. 2009, and references therein), peculiar infrared (IR) colors (Massaro et al. 2011; D'Abrusco et al. 2014, hereinafter Paper I), high optical polarization (see, e.g., Agudo et al. 2014; Pavlidou et al. 2014; Angelakis et al. 2016; Hovatta et al. 2016), and, not least, rapid and irregular variability (see, e.g., Homan et al. 2002) at all frequencies with uncorrelated amplitudes and different timescales ranging from minutes to weeks (Homan et al. 2002). Blazars can reach bolometric luminosities up to 10^{49} erg s^{-1} during γ-ray flaring states (Orienti et al. 2014).

The emission from blazars, according to the unification scenario of radio-loud AGNs, arises from a relativistic jet closely aligned along the line of sight that, in some cases, can outshine the host galaxy and the other AGN emission components (see, e.g., Blandford & Rees 1978; Urry & Padovani 1995).

A close connection between the γ-ray and IR properties of blazars has recently emerged from the investigation of the all-sky surveys carried out with the *Wide-Field Infrared Survey Explorer* (*WISE*; Wright et al. 2010) and *Fermi* satellites (D'Abrusco et al. 2012; Massaro et al. 2016). The observed correlations across more than 10 decades of frequency has been proven to be an extremely powerful tool to identify new γ-ray-emitting blazars among *Fermi* sources with unknown or uncertain lower-energy counterparts (Massaro et al. 2012a; D'Abrusco et al. 2013).

With a sky density of $\sim$0.1 sources deg^{-2}, blazars dominate the γ-ray sky in the MeV–TeV energy range and represent $\sim$40% of the sources in the Third *Fermi* Large Area Telescope (LAT) Source Catalog (3FGL; Acero et al. 2015; Massaro et al. 2015). Blazars are mainly divided into two subclasses based on their optical spectra: (i) BL Lac objects, characterized by featureless optical spectra or showing emission and/or absorption lines of equivalent widths (EW) $<$5 Å (Stickel et al. 1991; Falomo et al. 2014), and (ii) flat-spectrum radio quasars (FSRQs) with a typical quasar-like optical spectrum. Hereinafter, we adopt the nomenclature used in the ROMA-BZCat catalog

(Massaro et al. 2009, 2015), where BL Lacs and FSRQs are referred to as BZBs and BZQs, respectively.

The spectral energy distributions (SEDs) of blazars are characterized by two broad components, a low-energy one peaking between the IR and X-ray bands and a high-energy one whose emission ranges between the X-rays and the γ-rays. The former component is interpreted as synchrotron radiation from relativistic particles accelerated in a jet, while the component at higher energies, according to leptonic models, is due to inverse Compton emission with seed photons that can have different origins (for more details, see, e.g., Böttcher 2007, 2012). Hadronic models invoke the synchrotron emission by protons or secondary particles produced in proton–photon interactions (Dermer & Schlickeiser 1993; Mücke & Protheroe 2001; Murase et al. 2012, and references therein).

The BL Lac population is also divided, according to their SEDs, into "low-frequency peaked BL Lac objects" (LBLs), when the peak of the first component lies in the IR-to-optical energy range, and "high-frequency peaked BL Lac objects" (HBLs), when the synchrotron peak falls in the UV–to–X-ray energy range (Padovani & Giommi 1996). Another, more recent classification distinguishes blazars as low-synchrotron peaked, intermediate-synchrotron peaked, or high-synchrotron peaked (HSP) based on the peak frequency $\nu_{S,\mathrm{peak}}$ of the synchrotron component of their SEDs (Abdo et al. 2010; Ackermann et al. 2015). Here we will adopt the LBL/HBL subclassification for the BZBs, as it does not strictly depend on the exact location of the peak frequency.

The discovery of the peculiar *WISE* IR colors of blazars has been used to search for blazar-like sources within the positional uncertainty regions of the unidentified/unassociated γ-ray sources (UGSs) that could be their potential counterparts (see, e.g., Massaro et al. 2015). Several procedures based on *WISE* data have been developed to investigate the nature of the UGSs listed in all *Fermi* source catalogs, as well as to verify the nature of blazar candidates of uncertain type (BZUs; Massaro et al. 2012b; Cowperthwaite et al. 2013; Álvarez Crespo et al. 2016a). However, all of these methods require spectroscopic confirmation of the natures of the blazar candidates selected.

One of the largest sources of candidate blazars used to identify UGSs observed by the *Fermi* LAT has been the catalog of *WISE* Blazar-like Radio-Loud Sources (WIBRaLS; Paper I). This catalog contains *WISE* sources detected in all four *WISE* bands whose mid-IR colors are similar to those of confirmed *Fermi* blazars. WIBRaLS sources were also required to (a) have a radio counterpart from one of three major surveys, namely, the National Radio Astronomy Observatory's Very Large Array (VLA) Sky Survey (NVSS; Condon et al. 1998), the VLA Faint Images of the Radio Sky at Twenty-cm Survey (FIRST; White et al. 1997; Helfand et al. 2015), and the Sydney University Molonglo Sky Survey Source Catalog (SUMSS; Mauch et al. 2003); and (b) be radio-loud, that is, to have an observed ratio between radio and 22 μm mid-IR flux densities >3 (Paper I).

Since the publication of the WIBRaLS catalog, extensive optical spectroscopic campaigns whose goal is to verify the nature of WIBRaLS1 blazar candidates that can be spatially associated with γ-ray sources observed by *Fermi* have been carried out (see, e.g., Massaro et al. 2014, 2015; Paggi et al. 2014; La Mura et al. 2015; Landoni et al. 2015; Ricci et al. 2015; Álvarez Crespo et al. 2016a, 2016b, 2016c; Ajello et al. 2017a; Paiano et al. 2017a, 2017b, 2019; Peña-Herazo et al. 2017; Landoni et al. 2018; Marchesi et al. 2018; Marchesini et al. 2019). The total number of WIBRaLS candidate blazars that have been spectroscopically followed up and reported upon in any one of the papers listed above is, to date, 159, split into 126 candidate BZBs, 16 candidate BZQs, and 17 candidates with no spectral classification available (mixed). The analysis of the optical spectra confirmed that $\sim$93% of the candidate BZBs have featureless optical spectra typical of BL Lacs and $\sim$52% of the candidate BZQs show FSRQ spectra. Only $\sim$3%, $\sim$12%, and $\sim$11% of the spectra of observed candidate BZBs, BZQs, or mixed blazars cannot be classified as belonging to blazars, yielding a weighted average efficiency of the selection of $\sim$95%. Checks of spectra already published in the literature for 28 additional candidate blazars from WIBRaLS1 confirmed a BL Lac or FSRQ nature for 27 of them.

Since the publication of the first release of the WIBRaLS catalog (Paper I), new versions of some of the main data sets used to define the selection method used for the WIBRaLS catalog have been released.

1. The ROMA-BZCat, which contains the list of bona fide, spectroscopically confirmed blazars used to define the locus occupied by γ-ray-emitting blazars in the *WISE* color space, has reached its fifth release (Massaro et al. 2009). This release contains $\sim$3600 sources, versus $\sim$3050 sources in the version used by D'Abrusco et al. (2014).
2. The 3FGL (Acero et al. 2015) catalog of γ-ray sources detected by *Fermi* containing $\sim$5000 sources has also become available. This recent update to the catalog of *Fermi*-LAT sources is more than twice as large as the 2 yr (2FGL; Nolan et al. 2012) catalog ($\sim$2250 members) used to extract the first version of the WIBRaLS catalog.

These two new data sets jointly yield a larger sample of confirmed γ-ray blazars that can be used to more accurately characterize their *WISE* mid-IR properties and hence more effectively identify blazars that may be detected in the γ-ray energy range. In this paper, we describe a new release of the WIBRaLS catalog that, by taking advantage of these most recent data available, maximizes the legacy value of *WISE* observations for the investigation of blazars.

The completeness of the WIBRaLS catalog is a function of the blazar spectral class and decreases significantly for BL Lacs, which often are not detected in the 22 μm *WISE* band. The BZBs, in particular HBLs, have a lower detection rate in the [22] *WISE* band (Paper I), since their emission in the mid-IR at 22 μm may be lower than the limiting sensitivity in the fourth *WISE* band.

For this reason, in this paper, we will also present a new complementary catalog of candidate BZBs selected with a novel technique that employs the *WISE* colors obtained from the first three *WISE* bands only and has been applied to AllWISE sources not detected in *W4*. We focus only on the BZB spectral class for two main reasons: (i) the region of the IR color–color space occupied by BZBs is less contaminated by spurious IR sources than that of BZQs, and, (ii) during our campaign of spectroscopic follow-up of candidate BL Lacs selected with *WISE* colors, we found that a large fraction of UGSs and BZUs are classified as candidate BZBs, providing an

indication that they are the most elusive counterparts of *Fermi* sources (70.5% and 65.4%, respectively; see Massaro & D'Abrusco 2016).

The paper is organized as follows. In Section 2 we provide a brief introduction to the *WISE* and radio catalogs used to extract both samples of candidate blazars. Sections 3 and 4 describe the selection methods of the new WIBRaLS catalog and the catalog of BL Lac candidates selected using two *WISE* colors only, respectively. The comparison between the two catalogs presented in this paper and the literature is described in Section 5. Finally, our conclusions are summarized in Section 6.

We use cgs units unless otherwise stated, and spectral indices, α, are defined by flux density $S_\nu \propto \nu^{-\alpha}$, indicating as flat spectra those with $\alpha < 0.5$. The *WISE* magnitudes used here are in the Vega system and are not corrected for the Galactic extinction. As shown in our previous analyses (D'Abrusco et al. 2013, 2014), such correction affects only the magnitude at 3.4 μm for sources lying at low Galactic latitudes, and it ranges between 2% and 5% of the magnitude, thus not significantly affecting our results.

2. Data

2.1. IR Data

All of the candidate blazars discussed in this paper were sources extracted from images produced by the *WISE* space telescope (Wright et al. 2010). *WISE* has observed the whole sky from 2009 to 2011 in the four bands *W1, W2, W3*, and *W4* centered on 3.4, 4.6, 12, and 22 μm, respectively.

The AllWISE source catalog has superseded the previously available *WISE* All-Sky catalog; it was produced by combining *WISE* single-exposure images from the first two years of the mission with the post-cryogenic phase data (Mainzer et al. 2011) that observed the sky in three (*W1*, *W2*, and *W3*) and then only two (*W1* and *W2*) bands. The final result is a twofold improvement in the depth of coverage in the first two bands thanks to the additional observations that have increased the sensitivity of the stacked images and improved the photometric accuracy in all filters thanks to updated background measurements. The AllWISE sensitivities are 54, 71, 730, and 5000 μJy in the *W1, W2, W3*, and *W4* passbands, respectively, with angular resolutions of 6.″1, 6.″4, 6.″5, and 12″. Due to the *WISE* survey strategy, the limiting sensitivity of the catalog of sources extracted from the *WISE* images is not uniform on the sky (compare with Figure 8 of the Explanatory Supplement to the AllWISE Data Release Products[13]).

The AllWISE Source Catalog contains astrometry and photometry in the IR for 747,634,026 objects; only 25,882,082 of these sources (∼3.5%) were seen in all four bands, increasing up to 99,118,890 sources (∼13.3%) detected in the first three bands (*W1*, *W2*, and *W3* only). These two catalogs represent the parent samples for the updated WIBRaLS (Section 3) and the new catalog of BL Lac candidates (Section 4), respectively.

2.2. Radio Data

We have cross-matched the catalog of AllWISE sources according to the procedure described in Section 3.2 with the NVSS, FIRST, and SUMSS radio surveys. A brief description of each of these three radio surveys is given below.

1. The NVSS (Condon et al. 1998) is a 1.4 GHz continuum survey performed using the VLA and covering the entire sky north of −40° decl., i.e., 82% of the celestial sphere with a beam size of 45″ FWHM. The result is a catalog of over 1.8 million discrete sources brighter than $S \sim 2.5$ mJy in the entire survey.
2. FIRST (White et al. 1997; Helfand et al. 2015) is a project designed to produce the radio equivalent of the Palomar Observatory Sky Survey over 10,000 deg^2 of the north and south Galactic caps using the NRAO VLA. The beam size varies between 5.″4 FWHM for a circular beam and 6.″8 along the major axis for an elliptical shape as a function of the decl. of the observation. The survey area has been chosen to coincide with that of the Sloan Digital Sky Survey (SDSS; see, e.g., Gunn et al. 1998), and, at the $m_v \sim 23$ limit of SDSS, ∼40% of the optical counterparts to the FIRST sources are detected. At the 1 mJy source detection threshold, there are ∼90 sources deg^{-2}.
3. SUMSS (Mauch et al. 2003) is a radio imaging survey of the southern sky carried out with the Molonglo Observatory Synthesis Telescope (MOST) operating at 843 MHz with a beam size of ≈43″ FWHM. The catalog covers approximately 3500 deg^2 with decl. $\delta < -30°$, about 43% of the total survey area. The survey has a limiting peak brightness of 6 mJy beam^{-1} at decl. $\delta \leqslant -50°$ and 10 mJy beam^{-1} at $\delta > -50°$. SUMSS is therefore similar in sensitivity and resolution to the NVSS, with ∼7000 sources found in the overlap region.

3. The Second Release of the WIBRaLs Catalog

In this paper, a new release of the WIBRaLS catalog has been built up by following an improved version of the procedure described by Paper I and including new samples of confirmed blazars associated with *Fermi* γ-ray sources. Schematically, the steps we followed to extract the WIBRaLS catalog are the following.

1. We select *WISE* sources detected in all four *WISE* bands with IR colors similar to those of associated *Fermi* blazars (Section 3.1). We call these sources "*WISE* blazar-like sources."
2. The *WISE* blazar-like sources are positionally cross-matched with sources extracted from any of the radio surveys NVSS, SUMSS, and FIRST (Section 3.2), and only those with a radio counterpart are retained.
3. Among the WISE blazar-like sources with a radio counterpart, only radio-loud sources are selected as members of the WIBRaLS catalog (Section 3.3).

In the following, we provide descriptions of each step above.

3.1. WISE Color Selection of Blazar-like Sources

We define the blazar-like locus using the sample of confirmed *Fermi* blazars based on the fifth version of the ROMA-BZCat catalog (Massaro et al. 2015) and the 3FGL catalog (Acero et al. 2015) associated with AllWISE counterparts detected in all four *WISE* filters. This locus thus includes

[13] http://wise2.ipac.caltech.edu/docs/release/allwise/expsup/sec4_2.html

newly identified four-band sources and extends the locus presented in Paper I.

The BZCat v.5.0 contains 3561 bona fide blazars with spectroscopic confirmation. Optical spectra are also used to classify members of the BZCat as BZBs or BZQs, according to the total EW of all emission and absorption features, while blazars whose properties are intermediate between BZB and BZQ are tagged as uncertain (BZU), and other blazar-like objects whose emission is mostly contaminated by light from the host galaxy are labeled as BZGs.

All BZCat sources classified as BZU and BZG were discarded, leaving 1151 BZBs and 1909 BZQs. In order to spatially cross-match the positions of these BZCat sources with the AllWISE sources detected in the four filters, we adopted the maximum radial distance of $3\farcs3$ obtained by conservatively combining a nominal uncertainty of $1''$ on the radio positions of BZCat sources with a positional uncertainty in the *WISE W4* passband (see D'Abrusco et al. 2013 for details). This sample was then spatially cross-matched with γ-ray sources included in the 3FGL catalog (Acero et al. 2015), the latest release of sources detected by the LAT instrument on board NASA's *Fermi* spacecraft, based on the first 48 months of survey data. The cross-match has been performed by taking into account the position angles and the lengths of the semimajor and semiminor axes of the 95% confidence region of each *Fermi* source, available in 3FGL, and the positional uncertainty of the AllWISE counterparts of the BZCat sources. The final sample used to define the *WISE* three-dimensional locus consists of 901 confirmed γ-ray-emitting blazars, split in 497 BZBs and 404 BZQs, and is more than twice as large as the analogous list in Paper I, which contained 447 sources.

Following Paper I, we define a model of the locus in the three-dimensional principal component (PC) space generated by the three independent *WISE* colors *W1–W2* ([3.4]–[4.6]), *W2–W3* ([4.6]–[12]), and *W3–W4* ([12]–[22]). The locus is modeled as a set of three coaxial cylinders whose axes lie in the direction of the first PC (PC1). The two extremal cylinders are populated by blazars of similar spectral classes, namely, BZB and BZQ, while the intermediate cylinder contains significant ($\geqslant$25%) fractions of both BZBs and BZQs. The length along the PC1 axis of the two extremal cylinders is defined so that they contain at least 75% of the blazars classified as candidate BZBs and BZQs, while excluding the locus sources with a PC1 value smaller than the first percentile and larger than the 99th percentile of the distribution of locus PC1 coordinates. The mixed cylinder contains fractions of BZBs and BZQs that are each smaller than 75%. The radii of the three cylinders, which lie in the plane generated by PC2 and PC3 and orthogonal to PC1, are defined to contain 95% of the sources whose PC1 coordinates fall in each of the three cylinders. Sources located within the locus are selected on the basis of the value of their "score," a quantitative measure of the distance of a generic source to the locus model, defined as follows.

The *WISE* colors of a *WISE* source and the associated uncertainties are projected into the PC three-dimensional space, where they define an "uncertainty ellipsoid." The position and orientation of this ellipsoid—relative to the model of each cylinder separately—are used to calculate a numeric value defined between zero and 1. This normalized distance is then weighted by the volume of the error ellipsoid, so that two *WISE* sources placed in the same position relative to the locus model but with different uncertainties are assigned different scores. A more detailed description of the score and its properties can be found in Paper I.

Table 1
Values of the Score Thresholds $s_{5\%}$, $s_{20\%}$, $s_{60\%}$, and $s_{90\%}$ Used for the Extraction of the *WISE* Blazar-like Sources and to Define the Classes as Described in Section 3.1

	BZB-like	Mixed	BZQ-like
$s_{5\%}$ (D)	0.24	0.32	0.22
$s_{20\%}$ (C)	0.51	0.54	0.48
$s_{60\%}$ (B)	0.74	0.85	0.77
$s_{90\%}$ (A)	0.91	0.99	0.91

Note. These values are determined as the 5th, 20th, 60th, and 90th percentiles of the distribution of scores of the locus sample separately for BZB, mixed, and BZB cylinders in the locus model.

The score is also used to classify candidate blazars compatible with the model of the locus according to their reliability. All *WISE* sources with a nonzero score for either cylinder are ranked according to the decreasing compatibility with the locus model in the classes A, B, C, and D, defined by the 90th, 60th, 20th, and 5th percentiles of the score distribution for the sources of the locus sample. These classes are defined to facilitate quick prioritization of candidate blazars as targets of follow-up observation across sources of different spectral types (BZB-like, BZQ-like, or mixed) and regardless of the specific score distributions for each spectral type. Nonetheless, classes do not replace scores as a quantitative indicator of the degree of compatibility of each candidate blazar with the locus model in the *WISE* color space; all scientific analysis on the final list of WIBRaLS should be performed using scores. The lower 5% threshold corresponds to the fraction of locus sources that are located outside the locus model by definition. The values of the score thresholds used to define the three classes are reported in Table 1.

All sources with scores larger than the fifth percentile threshold, for any one of the three cylinders, are assigned the corresponding type (BZB, BZQ, or mixed) and selected as *WISE* blazar-like sources. The mixed type does indicate a specific spectral class, since the mixed cylinder contains comparable fractions of both BZBs and BZQs.

The total number of *WISE* blazar-like sources selected is 526,681, split into 156,506 BZB candidates ($\sim$30%) and 348,805 BZQ candidates ($\sim$60%), with the remaining 21,370 sources ($\sim$4%) located in the mixed region. The *WISE* blazar-like sources can also be split into 7807 class A sources ($\sim$1%), 27,986 class B sources ($\sim$5%), and 149,052 class C sources ($\sim$28%), with the remaining 341,836 ($\sim$65%) belonging to class D.

3.2. Radio Counterparts

Following Paper I, we determined the optimal radii for the association of the *WISE* blazar-like sources with their potential radio counterparts in the NVSS, SUMSS, and FIRST surveys.

We adopted a modified version of the procedure illustrated by Best et al. (2005) and Donoso et al. (2009). They computed the optimal radius for the spatial cross-match of NVSS and FIRST radio detections with optical sources in SDSS by setting a threshold on the fraction of spurious associations (i.e., the contamination) obtained for different values of the maximum cross-match radius. In this paper, similar to what was done in Paper I, the optimal association radius is indeed set as the radial

distance that provides a given fixed efficiency of the selection $e_{\rm thr} = 99\%$, corresponding to a contamination $c_{\rm thr} = 1\%$, where $c(\vartheta) = 100\% - e(\vartheta)$. The efficiency or purity of the selection is defined as the number of sources around real radio positions $n_{\rm real}(\vartheta)$ reduced by the number of sources around mock radio positions $n_{\rm mock}(\vartheta)$ and divided by the number of "real" matches.

We estimated $n_{\rm real}(\vartheta)$ by counting the number of *WISE* sources detected in all four bands within circular regions of radius ϑ between $0''$ and $60''$ centered on a sample of 5×10^4 sources randomly extracted from each of the three radio surveys. The value of $n_{\rm mock}(\vartheta)$ was calculated by averaging over 100 mock realizations of the coordinates of each real radio source, generated by moving the real position in a random direction and by a random radial distance in the $[60'', 120'']$ range.

The maximum cross-match radii evaluated for the NVSS and SUMSS surveys are $\vartheta_{\rm NVSS} = 10\farcs4$ and $\vartheta_{\rm SUMSS} = 7\farcs4$, respectively, identical to those determined for the first release of the WIBRaLS catalog. This approach does not work for the FIRST survey because of the very high density of FIRST sources. For this reason, we assume as an optimal search radius for FIRST the value previously determined, $\vartheta_{\rm FIRST} = 3\farcs4$ (Paper I), which was obtained by combining conservative estimates of the positional uncertainties of FIRST and AllWISE sources.

The number of *WISE* blazar-like sources associated with at least one radio counterpart in either of the three surveys within the maximum radial distances discussed above is 32,630, split into 18,903 with an NVSS counterpart, 1040 with a FIRST counterpart, and 3323 with a SUMSS counterpart. In order to exclude *WISE* sources associated with distinct radio sources associated with the emission of lobes of the same radio galaxy, we searched for and removed all duplicate radio sources whose positions would fall within $6'$ from each other. This radius matches the typical positional uncertainty of γ-ray sources detected by LAT in the 3FGL (Acero et al. 2015). In these cases, the AllWISE source with the largest score among all the duplicates was retained. After this step, the numbers of *WISE* blazar-like sources with a radio counterpart in the NVSS, FIRST, and SUMSS catalogs are 18,693, 10,227, and 3287, respectively, for a total of 32,207 sources. This sample includes 5547 sources with a counterpart from both the NVSS and FIRST surveys and 709 sources with one counterpart in NVSS and one in SUMSS The number of unique *WISE* blazar-like sources associated with a radio counterpart (i.e., the previous sample after removing sources with radio counterparts listed in two catalogs) is 25,951, where ∼72% (18,693) have an NVSS counterpart, ∼18% (4687) have a FIRST counterpart, and the remaining ∼10% (2578) are associated with a FIRST source. Moreover, 7101 sources (∼27%) are classified as candidate BZBs, 2186 (∼8%) are classified as mixed candidates, and the remaining 1664 (∼64%) are classified as candidate BZQs,[14] with 1366 class A (∼5%), 3302 class B (∼13%), 9265 class C (∼36%), and 12,018 (∼47%) class D sources.

3.3. Radio-loudness Selection

Blazars are radio-loud AGNs, but not every radio-loud AGN is a blazar. Blazars are generally hosted in elliptical galaxies, whose emission at radio frequencies is dominated by synchrotron emission from particles accelerated in the AGN relativistic jet pointed along the line of sight. In order to distinguish blazars from other radio sources, when lacking radio spectral information, we adopted the approach described in what follows. Padovani et al. (2011), as well as Bonzini et al. (2013), suggested that AGN-powered radio sources can be identified using q_{24}, a modified definition of the so-called q parameter (Helou et al. 1985), i.e., the logarithm of the ratio of far-IR to radio flux density, to overcome the dearth of accurate flux density measurements at the far-IR frequency. The q_{24} parameter is defined as

$$q_{24} = \log(S_{24\mu\rm m}/S_{1.4\rm GHz}), \quad (1)$$

where $S_{24\mu\rm m}$ is the observed flux density at 24 μm and $S_{1.4\rm GHz}$ is the flux density measured at 1.4 GHz. Following D'Abrusco et al. (2014), we adopted a similar criterion to select "radio-loud sources" among the *WISE* blazar-like sources with a radio counterpart by using the parameter q_{22}, defined as

$$q_{22} = \log(S_{22\mu\rm m}/S_{\rm radio}), \quad (2)$$

where the flux density in the 24 μm band of the Multi-band Imaging Photometer used on *Spitzer* is replaced by the *WISE W4* (22 μm) band. This approach is possible thanks to the similarities of the two wavebands (see Paper I for additional details). For the $S_{\rm radio}$ in Equation (2), we used the radio flux density at 1.4 GHz for sources with an NVSS or FIRST radio counterpart. Given the lack of flux measurement at 1.4 GHz for SUMSS sources, for those sources, we used flux densities at 843 MHz.

Due to the remarkable flatness of the radio spectra of blazars (see, e.g., Healey et al. 2007; Massaro et al. 2013d), replacing the flux density at 1.4 GHz with the same quantity at 843 MHz produces a small effect of the value of the q_{22} parameter, whose size was estimated using the sample of *WISE* blazar-like sources with a radio counterpart detected in both the NVSS and SUMSS (508 sources). The distribution of the difference between the values of q_{22} (1.4 GHz) and q_{22} (843 MHz) is fairly constant across the interval of q_{22} (1.4 GHz) covered by our sample, with $\Delta q_{22} \approx -0.07$, confirming a fairly flat radio spectrum for the sources in this sample. Based on this finding, for the *WISE* blazar-like sources associated with SUMSS counterparts only, we have used the corrected q_{22} value, defined as q_{22}' (843 MHz) = q_{22} (843 MHz) + Δq_{22}.

Both the q_{24} and q_{22} parameters show a dependence on the redshift of the source, as their values decrease for larger redshifts (Bonzini et al. 2013; D'Abrusco et al. 2014). Figure 1 shows the distribution of q_{22} values for the confirmed γ-ray-emitting blazars in the locus sample with reliable redshift measurements as a function of the redshift and color-coded according to their spectral classification from the BZCat. Locus sources (mostly BZBs) with uncertain or unknown redshifts were not used, reducing the number of locus members to 563 (split into 159 BZBs and 404 BZQs). In Figure 1, the same trend reported by Bonzini et al. (2013) and Paper I is observed. If redshift estimates were available for all *WISE* blazar-like sources associated with a radio counterpart, we could have determined different q_{22} thresholds in different redshift bins. Since redshifts are not available, we used fixed values of q_{22}.

In this paper, we improve the approach used in Paper I by determining different q_{22} thresholds for *WISE* blazar-like sources

[14] The selection of candidate BZQs using solely their *WISE* photometry can be contaminated by normal quasars, as they share the same region of the *WISE* color space (Wright et al. 2010). Also, the existence of radio counterparts to *WISE*-selected BZQ candidates alone, lacking radio spectral characterization, does not remove the degeneracy (Stern et al. 2005, 2012).

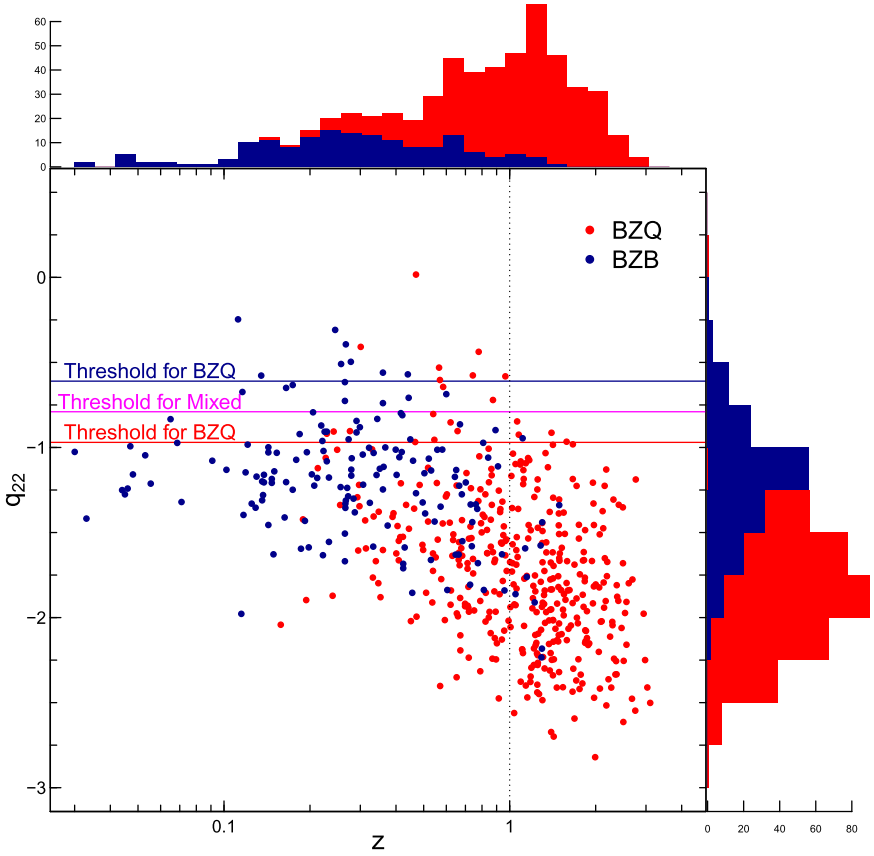

Figure 1. Scatter plot of the q_{22} values for the confirmed γ-ray-emitting blazars in the locus sample as a function of their redshifts reported in the BZCat (Massaro et al. 2015). The red, magenta, and blue horizontal lines show the values of the q_{22} thresholds used to select WIBRaLS sources among the *WISE* blazar-like sources with radio counterparts for *WISE*-based classes of candidate BZQs, mixed, and BZBs (see Section 3.3).

with radio counterparts classified as candidate BZQs, BZBs, and mixed. The thresholds for candidate BZBs and BZQs, calculated as 95% of the q_{22} distribution of all blazars in the locus sample classified as BZBs and BZQs, are $q_{22}^{\rm BZB} \leqslant -0.61$ and $q_{22}^{\rm BZB} \leqslant -0.97$, respectively. The threshold for mixed sources is set to the mean value of the thresholds for candidate BZQs and BZBs, $q_{22}^{\rm (mixed)} \leqslant -0.79$. These thresholds are shown as horizontal lines in Figure 1.

We evaluated the effect of the unknown underlying redshift distribution of the *WISE* blazar-like sources with radio counterparts on our selection based on fixed q_{22} thresholds. We followed the same strategy used in Paper I. We computed the q_{22} for all sources in the locus sample after varying their observed redshifts over an equally spaced grid covering the [0, 4] range with bins of 0.05 width, which includes the interval [0, $\sim$ 1.25] covered by the observed redshifts. We assumed a power-law SED with a slope constrained by the observed flux densities at 22 μm and 1.4 GHz. The fractions of candidate BZQs and BZBs that satisfy the q_{22} conditions based on the observed redshift distribution are $\sim$91% and $\sim$93%, respectively. These fractions are slightly lower than the $\sim$94% fraction of sources recovered with the $q_{22} \leqslant -0.5$ threshold used in Paper I.

The total number of *WISE* blazar-like sources with a radio counterpart that satisfies the radio-loudness criteria based on the q_{22} parameter and, thus, belong to the second release of the WIBRaLS catalog is 9541. The breakdown of the catalog according to *WISE* spectral type, class, and provenance of the radio counterpart is given in Table 2, while the basic parameters of a subset of sources in the catalog are displayed in Table 3. The number of sources of the locus sample of confirmed γ-ray-emitting blazars used to determine the WIBRaLS selection that are found in the final WIBRaLS2 is 666, $\sim$26% less than the original size of the locus sample (901 sources). The exclusion of these 235 locus sources is the result of (a) the definition of the *WISE* model (Section 3.1), which excludes 2% of the sources based on their location along the PC1 axis and 5% of each spectral class because the radii of the three cylinders are defined to contain 95% of the associated sources, and (b) the definition of the q_{22} thresholds (Section 3.3), which remove 5% of the remaining locus sources for each spectral class, by definition.

Table 2
Members of the WIBRaLS Catalog, Split According to Their *WISE* Spectral Types and Classes, and Provenance of the Radio Counterpart

	BZB-like	Mixed	BZQ-like	Total
Class A	55	5	61	121
Class B	273	124	317	714
Class C	1086	579	1746	3411
Class D	2330	0	2965	5295
NVSS	3024	557	4093	7664
FIRST	36	7	21	64
SUMSS	694	144	975	1813
Total	3744	708	5089	9541

Table 3
Sample of Rows of the Catalog of WIBRaLS Sources

AllWISE Name[a]	R.A.[b]	Decl.[c]	*W1–W2*[d]	*W2–W3*[e]	*W3–W4*[f]	s_{BZB}[g]	s_{MIX}[h]	s_{BZQ}[i]	Class[j]	Type[k]	Radio Counterpart[l]	S_{radio}[m]	q_{22}[n]
J000011.09–433316.4	0.0462203	−43.5545611	1.31	2.85	2.67	0.0	0.0	0.39	D	BZQ	SUMSS J000011.2–433317	70.9	−1.41
J000020.40–322101.2	0.0850076	−32.3503443	1.35	3.26	2.47	0.0	0.0	0.52	C	BZQ	NVSS J000020–322059	520.9	−1.94
J000029.07–163620.2	0.1211645	−16.6056221	0.39	2.01	2.45	0.53	0.0	0.0	C	BZB	NVSS J000029–163621	89.1	−1.24
J000047.05+312028.2	0.1960452	31.3411703	0.82	2.48	2.4	0.32	0.0	0.0	D	BZB	NVSS J000047+312027	46.4	−1.43
J000056.54–402206.4	0.235613	−40.368453	0.71	2.69	2.6	0.28	0.0	0.0	D	BZB	SUMSS J000056.7–402208	76.0	−1.36
J000101.04+240842.5	0.2543718	24.1451458	1.23	3.06	2.13	0.0	0.0	0.34	D	BZQ	NVSS J000101+240842	46.6	−1.26
J000105.29–155107.2	0.2720486	−15.8520035	1.18	3.42	2.14	0.0	0.0	0.33	D	BZQ	NVSS J000105–155106	347.5	−2.01
J000108.11-373857.1	0.2838199	−37.6492076	1.32	2.72	2.29	0.0	0.0	0.39	D	BZQ	SUMSS J000108.0–373901	23.1	−1.12
J000118.01–074626.9	0.3250683	−7.7741395	0.95	2.58	2.19	0.64	0.13	0.0	C	BZB	NVSS J000118–074626	208.4	−1.23
J000131.63+165413.8	0.3818138	16.9038342	1.21	2.92	2.45	0.0	0.0	0.59	C	BZQ	NVSS J000131+165416	63.1	−1.08
J000132.22+135258.4	0.3842501	13.8829081	1.07	3.0	2.48	0.0	0.0	0.23	D	BZQ	NVSS J000132+135258	74.2	−1.59
J000132.34+240230.3	0.3847546	24.0417769	0.85	2.14	1.84	0.81	0.0	0.0	B	BZB	NVSS J000132+240231	359.2	−1.28
J000132.74–415525.2	0.3864515	−41.9236926	0.68	2.17	2.09	0.48	0.0	0.0	D	BZB	SUMSS J000133.1–415526	11.6	−0.84
J000132.83+145607.9	0.3868025	14.9355453	0.92	2.85	2.77	0.0	0.1	0.31	D	BZQ	NVSS J000132+145609	314.6	−1.69
J000137.07+431543.9	0.4044828	43.2622002	0.72	2.61	2.32	0.76	0.0	0.0	B	BZB	NVSS J000137+431544	61.8	−0.9

Notes.
[a] *WISE* name.
[b] R.A. (J2000).
[c] decl. (J2000).
[d] *W1–W2 WISE* color.
[e] *W2–W3 WISE* color.
[f] *W3–W4 WISE* color.
[g] Score for the BZB region of the locus.
[h] Score for the mixed region of the locus.
[i] Score for the BZQ region of the locus.
[j] Class (see Section 3.1).
[k] Spectral type (see Section 3.1).
[l] Name of the radio counterpart.
[m] Radio flux density [mJy].
[n] Radio-loudness parameter q_{22}.
(This table is available in its entirety in FITS format.)

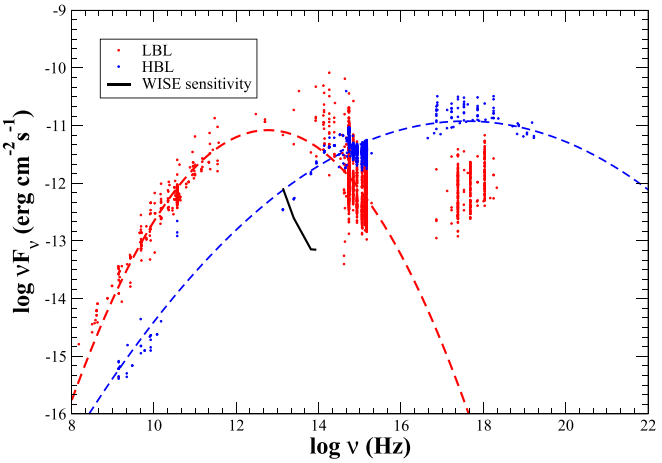

Figure 2. Historical SEDs of the two BZBs 1H 1426+428 (blue points), a TeV HBL, and AO 0235+164 (red points), a typical LBL (see Massaro et al. 2008a, 2008b, respectively). Dashed lines represent the best-fit log-parabolic functions used to describe their synchrotron components. The sensitivity limits in the four *WISE* bands are shown as a solid black line.

4. Catalog of *WISE* γ-Ray BL Lac Candidates

As mentioned briefly in Section 2.1, only ≈2.5% of the AllWISE sources are detected at 22 μm. For this reason, the WIBRaLS catalog, which requires its members to be detected in all four *WISE* bands, will certainly be incomplete for BZBs whose SEDs peak in the X-ray and are not bright enough to be detected in the *W4 WISE* band. This occurrence is schematically displayed in Figure 2, where the typical shapes of the SEDs of HBLs and LBLs are plotted together with the *WISE* sensitivity limits for the four *WISE* filters.

We designed a novel method that relies only on the colors obtained with the *W1*, *W2*, and *W3 WISE* bands to produce a list of candidate BL Lacs extracted from the AllWISE survey. The steps adopted for our procedure can be summarized as follows.

1. We select all AllWISE sources detected only in the first three *WISE* bands having IR colors similar to those of known *Fermi* BZBs belonging to the ROMA-BZCat v5.0.
2. From this sample, we further select only those sources with a radio counterpart in any of the NVSS, SUMSS, and FIRST radio surveys.
3. We identify as candidate BZBs sources whose values of the radio-to-IR flux density ratio are compatible with those of confirmed *Fermi* BL Lacs.

Details on these steps are given in the following sections.

4.1. WISE *Color Selection of BZB-like Sources*

The training set used to identify the *WISE* mid-IR colors of BL Lac objects was built by selecting all of the *Fermi* sources belonging to the 3FGL and associated with BZBs in the latest release of the ROMA-BZCat catalog (Massaro et al. 2015). We only considered sources whose AllWISE counterparts are not detected in the *W4* band. The total number of unique sources in the training set is 93. Among these sources, 34 are associated with an NVSS radio counterpart only, three are associated with a FIRST source only, and the remaining 56 have both an NVSS and FIRST counterpart.

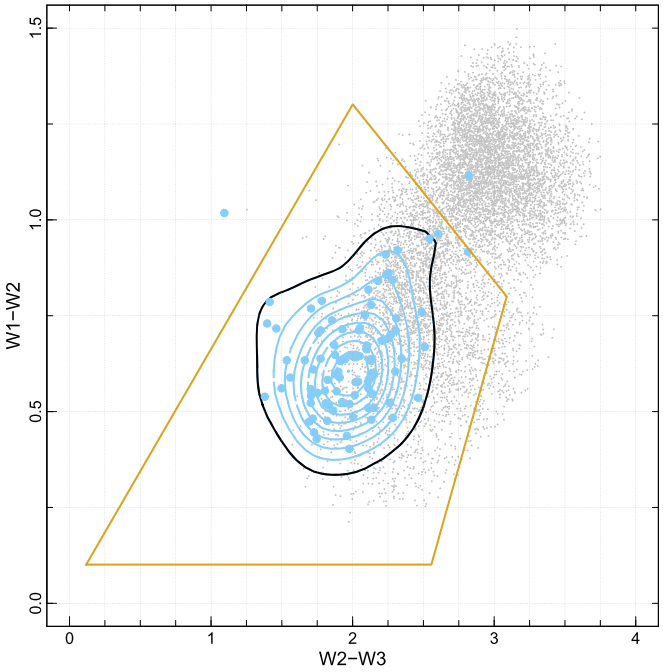

Figure 3. *WISE W2–W3* vs. *W1–W2* color–color diagram. The 93 sources in the training set are shown by light blue circles, and the black line is the contour containing 90% of the sources in the training set and used to select the candidate KDE BL Lacs. Sources in the WIBRaLS catalog are displayed in the background for comparison (small gray circles). The yellow polygon shows the region in the *WISE* color plane where sources from the 2WHSP catalog are located (Chang et al. 2017; see Section 5.1).

We selected *WISE* sources with IR colors similar to those of our training set by adopting the same procedure used in previous analyses (see, e.g., Massaro et al. 2011, 2013a; Paggi et al. 2013) based on the kernel density estimation (KDE). The KDE is a nonparametric procedure that estimates the probability density function (PDF) of a multivariate distribution with no assumption of the properties of the parent population. The KDE depends on only one parameter, i.e., the bandwidth of the kernel of the density estimator, which is qualitatively analogous to the window size for a one-dimensional running average.

We applied the KDE to the two-dimensional distribution of training set sources in the *WISE W2–W3* versus *W1–W2* color–color plane to determine its PDF. Then, we selected IR sources in the AllWISE catalog not detected in the *W4* passband and detected in the other three filters, whose colors are located within the isodensity contour enclosing 90% of the BL Lac training set. Only sources whose color uncertainty ellipses are entirely contained within the 90% isodensity contour were retained. Figure 3 shows the distribution of the training set in the *WISE* color plane, together with the isodensity contours determined by the KDE method, with the 90% contour displayed as a thick black line. The projections on this color–color diagram of the WIBRaLS2 catalog are also shown for reference.

The total number of *WISE* sources extracted by applying this method is ∼14,406, corresponding to ∼0.01% of the parent sample of AllWISE sources not detected only in *W4*.

4.2. *Radio Counterparts*

We further select possible BL Lac candidates by searching for radio counterparts of the sample of sources selected based

Table 4
Breakdown of the Number of *WISE* Sources Identified as BL Lac Candidates at Each Step of the Selection Described in Section 4, Split by Provenance of the Radio Counterparts

	NVSS	FIRST	SUMSS	Total
WISE selection	10,166	5532	2128	17,826
Duplicates removal	10,166	2099	1680	13,945
Close sources removal	100,084	2049	1671	13,804
q_{12} selection	5310	327	305	5942
$\|\|b\|\|$ selection	4947	327	305	5579

on their *WISE* colors. This procedure obviously misses "radio-weak BL Lacs," but to date, they are extremely rare, and their associations with *Fermi* sources have not yet been verified (Massaro et al. 2017; Bruni et al. 2018).

We cross-matched the color-selected *WISE* sources with the radio surveys NVSS, SUMSS, and FIRST using the same maximum association radii established as described in Section 3.2. We found a total of 17,826 sources with at least one radio counterpart: 5532 are associated with a FIRST source within $3\farcs4$, 10,166 with an NVSS source within $10''$, and the remaining 2128 with a SUMSS source within $7\farcs4$ (see Table 4). After removing from our list sources with SUMSS or FIRST counterparts that are also associated with an NVSS source, there remain 2099 *WISE* sources with a unique FIRST counterpart, 1680 *WISE* sources with a unique SUMSS counterpart, and the 10,166 sources associated with an NVSS radio source, for a total of 13,945 sources. Similar to what was done for the WIBRaLS catalog in Section 4.2, in order to avoid possible contamination from radio lobes originating from radio galaxies, we also checked for sources whose radio counterpart is closer than $6'$ to another radio source, and, for FIRST radio counterparts only, sources with side-lobe probability $\geqslant 0.05$. These constraints reduced the number of sources to 2049 with a unique FIRST counterpart, 1671 associated with a unique SUMSS source, and 10,084 with a radio counterpart in NVSS, for a total of 13,804 candidates.

4.3. IR-to-radio Ratio Selection

The last step of the procedure to select *WISE* BL Lac candidates is based on the characterization of the distribution of their IR-to-radio ratios q_{12}, similar to the q_{22} parameter used to select WIBRaLS sources (Section 3.2). We define the parameter q_{12} as

$$q_{12} = \log(S_{12\mu\mathrm{m}}/S_{\mathrm{radio}}), \quad (3)$$

i.e., the logarithm of the ratio between the *WISE* flux density measured in the *W3* passband and the radio flux density. The flux density at 20 cm has been used to calculate the q_{12} of sources with a unique counterpart in the NVSS and FIRST surveys. Given the flatness of the radio spectrum of BL Lacs (Healey et al. 2007; Massaro et al. 2013a) and our estimate of $\Delta q_{22} \approx -0.07$ for the *WISE*-selected sources with both SUMSS and NVSS radio counterparts (see Section 3.3), we assume a flat spectrum ($\alpha_{\mathrm{radio}} = 0$) and use the flux density at 36 cm to calculate the q_{12} parameter for sources with SUMSS counterparts.[15]

[15] We estimate that for radio spectra with $\alpha_{\mathrm{radio}} = \pm 0.1$, the effect on the values of q_{12} (843 MHz) calculated at 36 cm for SUMSS counterparts would be a factor ranging from ≈0.95 to ≈1.05. In the case of a much larger spectral index, $\alpha_{\mathrm{radio}} = 0.5$, the corrective factor would still be ≈0.77.

We consider BL Lac candidates those sources whose q_{12} values are consistent with the observed q_{12} distribution of the training set sources. The q_{12} values for sources with a FIRST or NVSS radio counterpart (59 and 90, respectively) have been used separately to determine the intervals of acceptable q_{12} values for both surveys, as in both surveys' flux densities are measured at the same wavelength (20 cm).

Figure 4 shows the distributions of the q_{12} values of the BL Lac training set sources (light blue histograms), control samples including random *WISE* sources with radio counterparts (filled gray histograms), and candidate BL Lacs selected according to their *WISE* colors as described in Section 4.1 (dashed gray histograms). FIRST (upper panel), NVSS (middle panel), and SUMSS (lower panel) radio counterparts are shown separately; the light blue histogram is missing from the SUMSS panel, as no source in the training set has a radio counterpart from the SUMSS survey. It is also interesting to notice that the peaks of the distributions of q_{12} values for the control sample and the *WISE*-selected candidates with SUMSS radio associations (lower panel in Figure 4) are significantly shifted toward smaller values of q_{12} relative to the NVSS and FIRST distributions. This difference is due to the relative shallowness of the SUMSS survey, whose sensitivity allows the detection of sources with a minimum density flux at 36 cm $S_{\mathrm{radio}}^{\mathrm{SUMSS}}$ (36 cm) = 5 mJy, larger than the ∼2 and ∼0.2 mJy for NVSS and FIRST, respectively.

We defined the lower and upper limits of the q_{12} values used to select the candidate BL Lacs as the 10th and 90th percentiles of the q_{12} distribution of the training set (red lines in Figure 4). The q_{12} intervals used to select the candidates are between −1.85 and −1 for NVSS training set sources and −1.64 and −1.01 for sources with FIRST counterparts. Given the lack of training set BL Lacs with SUMSS counterparts, we have conservatively defined the upper and lower thresholds for the q_{12} selection of SUMSS BL Lac candidates as the highest and lowest values of the lower and upper thresholds on the q_{12} distribution of training set sources with a FIRST or NVSS counterpart, respectively. As a result, the interval of allowed q_{12} values for SUMSS counterparts ranges between −1.64 and −1. After applying the q_{12} selections to the sample of 13,804 *WISE* radio-selected sources, we obtain 5941 candidates, split into 327 associated with a FIRST source, 5310 with an NVSS counterpart, and 305 associated with a SUMSS source.

Then, as a final step, we discarded all sources in the catalog located at Galactic latitudes $|b| < 10\,^{\circ}$, since γ-ray sources at low galactic latitudes suffer from a higher detection threshold due to a higher Galactic diffuse emission background (Ackermann et al. 2015). This constraint reduces the total number of sources in the catalog of KDE-selected BL Lac candidates to 5579, due to the exclusion of 363 sources with an NVSS radio counterpart. In what follows, the sources in the catalog of KDE-selected candidate BL Lacs will be called KDEBLLACS. The breakdown of the number of BL Lac candidates selected at different stages of the procedure as a function of the different radio surveys is displayed in Table 4, while the properties available for a sample of sources in the final KDEBLLACS catalog are shown in Table 5.

5. Discussion

The full characterization of the two catalogs presented in this paper would require optical spectroscopic follow-up observations to confirm the nature of the candidates and will be discussed in a future paper. In this section, we examine the global spatial

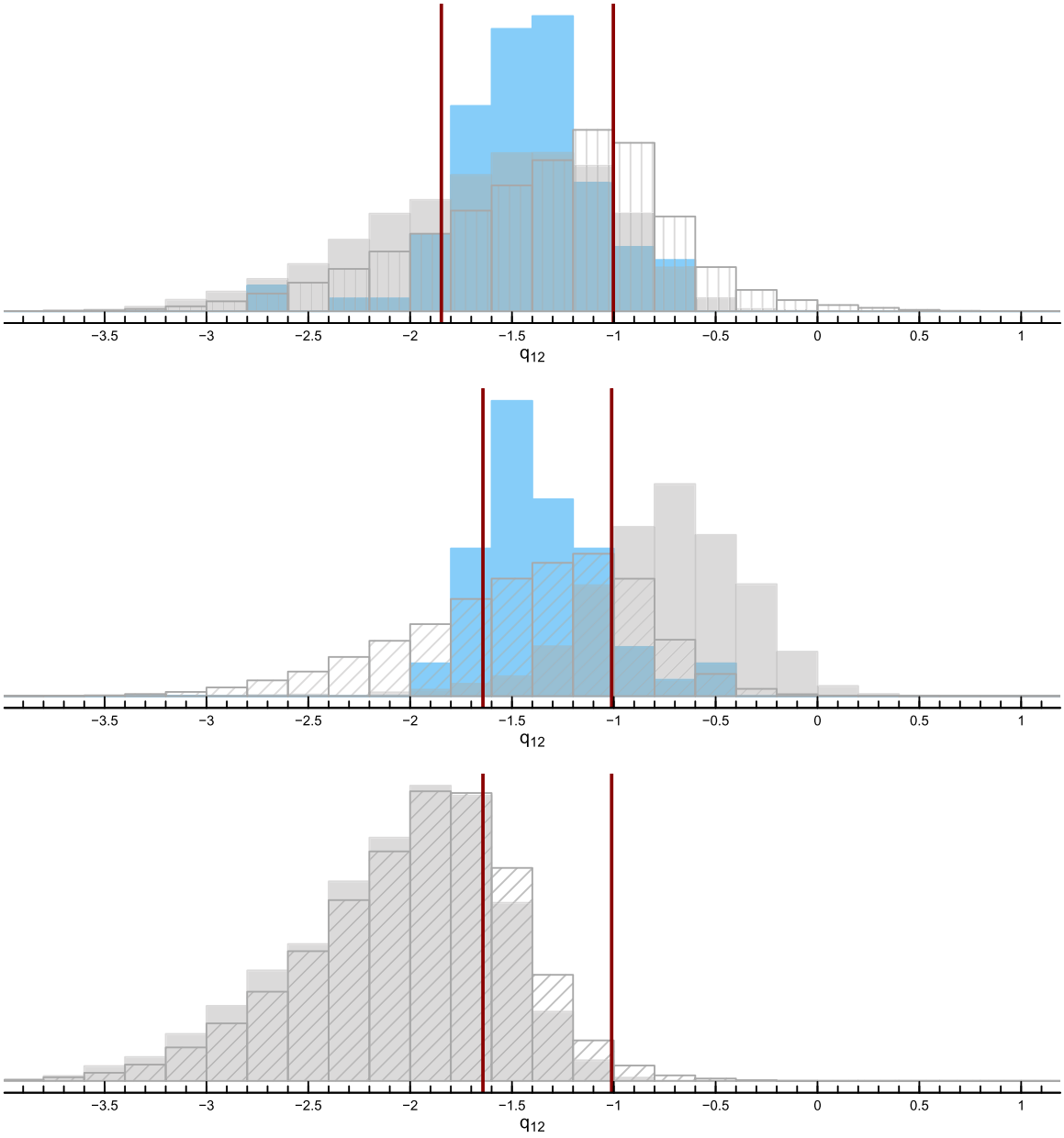

Figure 4. Upper panel: the light blue histogram shows the distributions of q_{12} values for confirmed γ-ray-emitting BL Lacs (training set sources for the KDE candidate BL Lacs) with a radio counterpart in the FIRST radio surveys. The filled and dashed gray histograms show the q_{12} distributions for a random sample of *WISE* sources associated with a FIRST counterpart and the *WISE* color-selected candidate KDE BL Lacs, respectively. Middle panel: same as upper panel for NVSS radio counterparts. Lower panel: q_{12} distributions for a random sample of *WISE* sources associated with a SUMSS radio source and *WISE* color-selected candidate KDE BL Lacs (no training set sources with SUMSS radio counterparts are available). In all panels, vertical red lines display the 10th and 90th percentiles of the q_{12} distribution of the training set used to select the final sample of sources in the KDEBLLACS catalog (see Section 4.3).

and *WISE* photometric properties of the WIBRaLS2 and KDEBLLACS catalogs and discuss how they compare with the most recent catalogs of *Fermi* γ-ray sources.

The Aitoff projections of the sky positions in galactic coordinates of the WIBRaLS2 and KDEBLLACS catalogs are shown in Figure 5. The coverage of the WIBRaLS2 catalog is mostly uniform across the sky (left panel in Figure 5), with the exception of a region along the galactic plane where radio sources are not available from any of the three surveys used. Two regions of higher density can be observed where the FIRST and SUMSS surveys overlap with the NVSS coverage, respectively, north and south of the Galactic plane. In the right panel, the sky distribution of the KDEBLLACS catalog prominently features a lower density of sources associated with SUMSS radio counterparts and the lack of sources due to the Galactic latitude selection described in Section 4.3.

It is interesting to compare the regions of the *WISE* color space occupied by the WIBRaLS2 and KDEBLLACS catalogs. The location of the sources belonging to the above catalogs in the *WISE* color space is displayed in Figure 6. The two samples occupy partially overlapping but distinct regions of the three-dimensional *WISE* color space. Since KDEBLLACS are not detected in the *W4* passband by definition, their positions along the *W3–W4* axis cannot be established, but the three-dimensional volume of the space potentially occupied by these sources can be determined by using the upper limits on their

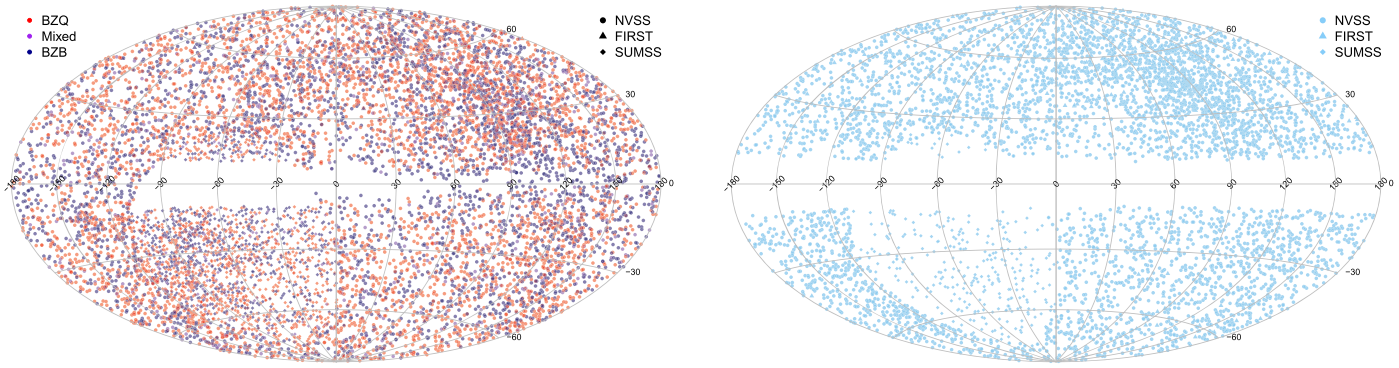

Figure 5. Left panel: Aittof projection of the distribution in galactic coordinates of the WIBRaLS2 sources. The provenance of the radio counterpart and *WISE* spectral class of the candidate blazars are encoded in the shape and color of the symbols, respectively. Right panel: Aitoff projection of the distribution in galactic coordinates of the BL Lac candidates selected with the KDE method. The provenance of the radio counterpart is encoded in the shape of the symbols.

Table 5
Sample of Rows of the Catalog of KDEBLLACS

AllWISE Name[a]	R.A.[b]	Decl.[c]	*W1*–*W2*[d]	*W2*–*W3*[e]	Radio Name[f]	S_{20cm}[g]	q_{12}[h]
J000007.63+420725.5	0.0318093	42.1237527	0.35	**1.92**	NVSS J000007+420722	18.2	−1.5
J000010.29–363405.2	0.042887	−36.5681267	0.53	**2.33**	NVSS J000010–363407	6.2	−1.3
J000056.22–082742.0	0.2342813	−8.4616809	0.43	**1.94**	NVSS J000056–082747	14.4	−1.6
J000116.37+293534.5	0.3182368	29.5929424	0.61	**2.46**	NVSS J000116+293534	3.5	−1.02
J000126.44+733042.6	0.3601711	73.5118347	0.77	**2.22**	NVSS J000126+733042	23.6	−1.63
J000137.86–103727.3	0.4077672	−10.6242584	0.40	**2.07**	NVSS J000137–103727	10.2	−1.41
J000147.28+455015.2	0.4470018	45.8375759	0.78	**1.91**	NVSS J000147+455016	4.2	−1.22
J000236.06–081532.4	0.6502775	−8.2590058	0.71	**2.11**	NVSS J000236–081533	28.3	−1.61
J000302.99–105638.1	0.7624893	−10.9439389	0.67	**2.36**	NVSS J000302–105637	18.2	−1.61
J000311.94–070144.3	0.7997588	−7.0289838	0.61	**1.98**	FIRST J000311.9–070144	4.17	−1.01

Notes.
[a] *WISE* name.
[b] R.A. (J2000).
[c] decl. (J2000).
[d] *W1*–*W2 WISE* color.
[e] *W2*–*W3 WISE* color.
[f] Name of the radio counterpart.
[g] Radio flux density [Jy].
[h] Radio-loudness parameter q_{12}.
(This table is available in its entirety in FITS format.)

W4 brightness (i.e., lower limits on their *W4* magnitude) available in the AllWISE catalog.

The two catalogs of blazar candidates described in this paper are complementary because their members can differ in spectral properties (see discussion in Section 4) and brightness. Figure 7, which displays the histograms of the magnitude values for the three *WISE* filters *W1*, *W2*, and *W3* for the WIBRaLS2 and KDEBLLACS samples together, confirms that the KDE-based method selects sources that are increasingly fainter than those in the WIBRaLS catalog as the wavelength increases going from filter *W1* to *W3*.

5.1. Comparison with the Literature

One of the main goals of the production of catalogs of candidate blazars, like the two discussed in this paper, is the discovery of multiwavelength counterparts of UGSs observed by *Fermi*. While the thorough analysis that is necessary to reliably associate low-energy candidate blazars with UGSs (see, for example, D'Abrusco et al. 2013; Massaro et al. 2015; Schinzel et al. 2015) is beyond the goals of this paper, as a consistency check and in order to assess the potential of the two catalogs discussed here to improve the characterization of the currently known γ-ray sources, we compared the WIBRaLS2 and KDEBLLACS catalogs with the most recent catalogs of sources detected by *Fermi* LAT.

We spatially cross-matched the WIBRaLS2 catalog with the 3FGL catalog (Acero et al. 2015) using the 98% elliptical uncertainty regions for 3FGL sources and a fixed positional uncertainty of 1″ on the WIBRaLS2 radio coordinates. We found a total of 1049 matches, including the 666 sources in the locus sample selected as WIBRaLS2 members (see Section 3.3). Among the remaining 373 sources, 49 are unassociated; the 320 sources that are associated or identified with a known multiwavelength counterpart in 3FGL are all classified, according to the CLASS1 parameter in 3FGL (Acero et al. 2015), as BL Lacs, FSRQs, or BZUs (blazar candidate of Uncertain type), except for three radio galaxies and three soft-spectrum radio quasars. The cross-match between the KDEBLLACS catalog and 3FGL, using the same positional uncertainties, returned 186 matches (all distinct from the WIBRaLS2 cross-matches), with 57 unassociated sources. About 95% of the remaining 131 3FGL

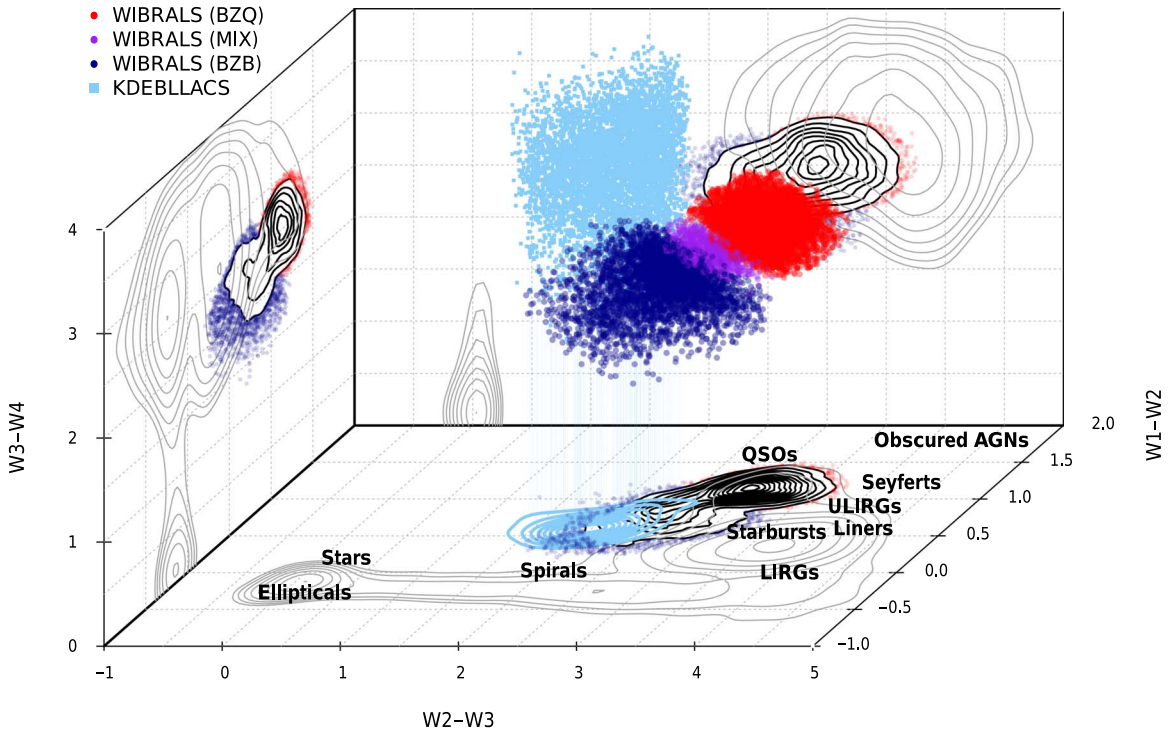

Figure 6. Distribution of the WIBRaLS2 and KDEBLLACS catalogs in the three-dimensional *WISE* color space. WIBRaLS2 sources are color-coded according to their *WISE* spectral classification, while the three-dimensional positions of the KDEBLLACS sources (light blue), given their nondetection in the *W4* filter, are visualized by using the lower limit in the *W4* magnitude and by segments originating from these points and delimiting the three-dimensional volume in the color space where these sources may actually be located. The isodensity contours of the distributions of the WIBRaLS2 (black) and KDEBLLACS (light blue) samples are shown in the *W2–W3* vs. *W1–W2* plane, while the gray lines on the three color–color planes represent the projected isodensity contours associated with 10 log-spaced levels of a sample of *WISE* random sources (including sources both detected and not detected at 22 μm). The approximate locations of different classes of sources in the *W2–W3* vs. *W1–W2* color–color plane according to Wright et al. (2010) are also shown for guidance.

sources cross-matched with a KDEBLLACS source that are associated or identified are classified as BZUs or BL Lacs, according to the 3FGL CLASS parameter. The total number of unique cross-matched sources from either the WIBRaLS2 or KDEBLLACS catalogs increases to 1757 (1404 and 353, respectively) when the preliminary LAT 8 yr Point Source List (FL8Y; which contains a total of 5523 γ-ray sources)[16] is used, for a total of 152 unassociated sources. Out of the 1605 associated or identified sources, ∼99% are classified as either BL Lacs, FSRQs, or BZUs.

Following the same approach described above, we also cross-matched the WIBRaLS2 and KDEBLLACS catalogs with the Third Catalog of Hard *Fermi*-LAT Sources (3FHL; Ajello et al. 2017a). The spatial cross-match returns a total of 807 distinct matches, split into 647 from WIBRaLS2 and 160 from KDEBLLACS, with 33 unassociated 3FHL sources and the remaining 774 composed of BL Lacs (520, ∼68% of the total), and BZUs (∼16% of the total). The 83% of the WIBRaLS2 members cross-matched with 3FHL sources are classified as BZB or mixed candidates based on their *WISE* colors.

It is also useful to compare the two catalogs of candidate blazars presented in this paper with the largest catalog of candidate HSPs available in the literature to date, namely, the second *WISE* High Synchrotron Peaked Blazar (2WHSP) catalog (Chang et al. 2017), with 1691 entries. The 2WHSP is an expansion of the 1WHSP catalog (Arsioli et al. 2015) and contains HSP candidates drawn from the AllWISE catalog that can be associated with radio and X-ray counterparts. The 2WSHPs candidates are further selected by requiring that their radio-to-IR and IR–to–X-ray broadband spectral slopes are consistent with those of known, confirmed HSP sources (Chang et al. 2017) and that the peak frequency of the synchrotron emission component of their SEDs $\nu_{\rm peak}$ is $>10^{15}$ Hz (Chang et al. 2017). The 2WHSP contains 1691 unique candidates or confirmed HSPs: 460 of these sources are associated with AllWISE sources detected in four bands, and 717 sources are associated with sources detected in the first three (*W1*, *W2*, and *W3*) filters. The remaining sources cannot be compared to the catalogs discussed in this paper because they are not detected in both the *W3* and *W4* passbands. We determined that 248 of the 460 2WSHP sources detected in all AllWISE filters are also in the new WIBRaLS catalog, while 267 of the 717 sources not detected in *W3* have been selected as KDEBLLACS. The main cause of difference between our catalogs and the 2WHSP is the maximum spatial radius used to cross-match AllWISE sources with radio counterparts from one of the three radio surveys, FIRST, NVSS, and SUMSS. Chang et al. (2017) reported that radio counterparts were selected within 0.′3 and 0.′1 for the NVSS/SUMSS and FIRST catalogs, respectively. These radii are significantly larger than the radii used in this catalog, discussed in Sections 3.2 and 4.2 (10.″4, 3.″4, and 7.″4 for NVSS, FIRST, and SUMSS, respectively). As a consequence, only 311 AllWISE sources with a unique radio counterpart contained in the sample used to extract the KDEBLLACS can also be found in the 2WSHP catalog. Another possible source of the difference between the KDEBLLACS and 2WHSP catalogs is the extent of the region in the *WISE* color–color diagram where 2WHSP sources are

[16] https://fermi.gsfc.nasa.gov/ssc/data/access/lat/fl8y/

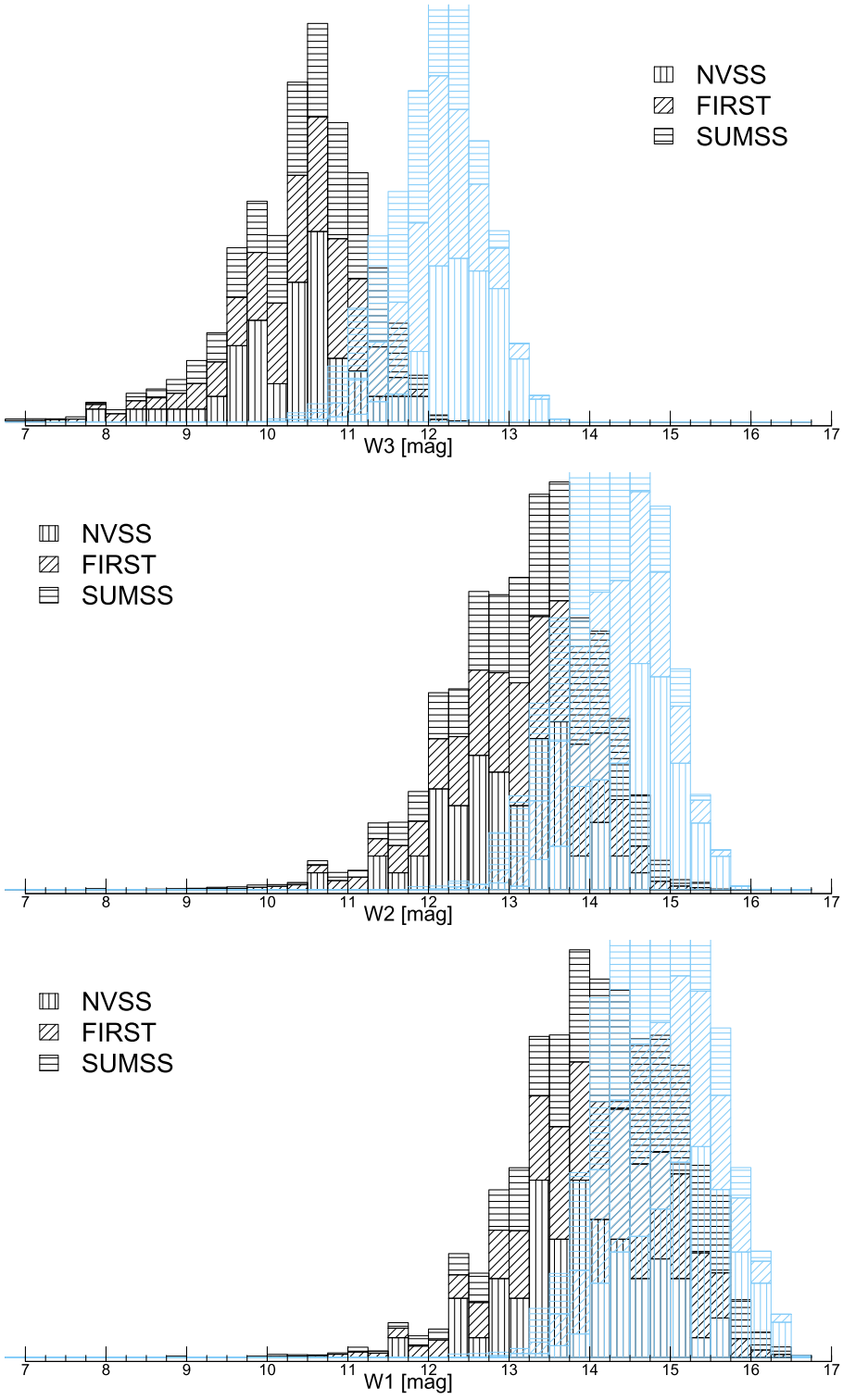

Figure 7. Distribution of magnitudes in the *W1* (lower panel), *W2* (middle panel), and *W3* (upper panel) *WISE* filters for WIBRaLS2 (black histograms) and KDEBLLACS (light blue histogram) candidate blazars, broken down by provenance of the radio counterpart.

located, which is significantly larger than the area from which the BL Lac candidates are selected (see Figure 3).

5.2. Comparison with the WIBRaLS1 Catalog

The second release of the WIBRaLS catalog, WIBRaLS2, described in this paper, contains 5025 candidate blazars also found in the first WIBRaLS (WIBRALS1) catalog (Paper I). Of the total 7885 members of WIBRALS1, 2830 sources are not included in WIBRaLS2 because their q_{22} values (for $\sim$95% of them) are larger than the new, more stringent thresholds adopted for BZQs in WIBRaLS2 (see Section 3.3). The increase in the size of the training set of confirmed γ-ray blazars used to define the WIBRaLS locus has led to an

increase of the volume in *WISE* color space that has produced 4711 sources in WIBRaLS2 not included in WIBRaLS1.

6. Summary and Conclusions

In this paper, we present two new catalogs of blazar candidates, selected on the basis of their *WISE* mid-IR colors, association with a radio counterpart, and radio-loudness. These new catalogs contain a combined total of 15,196 candidate blazars, including both candidate FSRQs and BL Lacs, distributed on ∼90% of the sky.

The second, enhanced release of the WIBRaLS catalog supersedes the original WIBRaLS1 (Paper I) catalog, which has been extensively employed to associate *Fermi* unidentified sources with their low-energy counterparts. WIBRaLS2 contains candidate blazars drawn from AllWISE sources detected in all four *WISE* passbands with colors similar to those of spectroscopically confirmed, γ-ray-emitting blazars that are associated with radio counterparts and identified as radio-loud. Spectral classification as candidate BZBs, BZQs, or mixed blazars, following the ROMA-BZCat (Massaro et al. 2015) terminology and derived from the *WISE* color properties, is also provided. WIBRaLS2 contains 9541 candidate blazars, an ∼25% increase over the first version of WIBRaLS.

The KDEBLLACS catalog complements WIBRaLS2 by identifying BL Lac candidates that, because of their typical low IR-to-radio ratios and/or *WISE* brightness (cf. HBLs), have gone undetected in the *W4 WISE* filter and, as a consequence, cannot be considered for selection in WIBRaLS2. The KDEBLLACS members are required to be detected in the three *WISE* filters, *W1*, *W2*, and *W3*, and are selected based on their positions in the *W2–W3* versus *W1–W2 WISE* color–color diagrams using the KDE technique. They are also associated with a radio counterpart and identified as radio-loud according to the q_{12} radio–to–mid-IR spectral parameter. We select 5579 sources in the KDEBLLACS.

Previous samples of candidate blazars selected on the basis of the IR colors, eventually combined with radio and/or multi-frequency observations (see, e.g., Massaro et al. 2013b, 2016; Arsioli et al. 2015; Maselli et al. 2015), have been used by the *Fermi*-LAT collaboration for the preparation of the 3FGL, the Third Catalog of Active Galactic Nuclei (3LAC; Ackermann et al. 2015), and the Second and Third Catalogs of Hard *Fermi*-LAT Sources (2FHL and 3FHL; Ackermann et al. 2016; Ajello et al. 2017a, respectively).

This work will contribute to a more comprehensive understanding of the diverse and fascinating γ-ray sky as observed by *Fermi*. In particular, the community will benefit from the WIBRaLS2 and KDEBLLACS catalogs of candidate blazars presented in this paper and the subsequent programs of follow-up spectroscopic observations needed to confirm their nature and, possibly, determine their redshifts by using them to (i) improve our knowledge of the luminosity function of BL Lacs (see, e.g., Ajello et al. 2014); (ii) select potential targets for the Cerenkov Telescope Array (CTA), as shown by Massaro et al. (2013e) and Arsioli et al. (2015); (iii) obtain more stringent limits on the dark matter annihilation in subhalos (see, e.g., Zechlin & Horns 2012; Berlin et al. 2014); (iv) search for counterparts of new flaring γ-ray sources (see, e.g., Bernieri et al. 2013) and high-energy neutrino emission (see, e.g., IceCube Collaboration et al. 2018); (v) test new γ-ray detection algorithms (see, e.g., Campana et al. 2015, 2016, 2017); and (vi) finally, perform population studies of the remaining UGSs (see, e.g., Acero et al. 2013).

R.D'A. is supported by NASA contract NAS8-03060 (Chandra X-ray Center).

The work of F.M. and A.P. is partially supported by the "Departments of Excellence 2018-2022" grant awarded by the Italian Ministry of Education, University and Research (MIUR; L. 232/2016) and made use of resources provided by the Compagnia di San Paolo for the grant awarded on the BLENV project (S1618_L1_MASF_01) and by the Ministry of Education, Universities and Research for grant MASF_FFABR_17_01. F.M. also acknowledges a financial contribution from the agreement ASI-INAF n.2017-14-H.0, while A.P. acknowledges the financial support of the Consorzio Interuniversitario per la fisica Spaziale (CIS) under the agreement related to grant MASF_CONTR_FIN_18_02.

F.R. acknowledges support from FONDECYT Postdoctorado 3180506 and CONICYT project Basal AFB-170002.

V.C. is partially supported by CONACyT research grant 280789.

This research has made use of data obtained from the high-energy Astrophysics Science Archive Research Center (HEASARC) provided by NASA's Goddard Space Flight Center; the SIMBAD database operated at CDS, Strasbourg, France; and the NASA/IPAC Extragalactic Database (NED) operated by the Jet Propulsion Laboratory, California Institute of Technology, under contract with the National Aeronautics and Space Administration. Part of this work is based on the NVSS (NRAO VLA Sky Survey). The National Radio Astronomy Observatory is operated by Associated Universities, Inc., under contract with the National Science Foundation and on the VLA low-frequency Sky Survey (VLSS). The Molonglo Observatory site manager, Duncan Campbell-Wilson, and the staff, Jeff Webb, Michael White, and John Barry, are responsible for the smooth operation of the Molonglo Observatory Synthesis Telescope (MOST) and the day-to-day observing program of SUMSS. The SUMSS survey is dedicated to Michael Large, whose expertise and vision made the project possible. The MOST is operated by the School of Physics with the support of the Australian Research Council and the Science Foundation for Physics within the University of Sydney. This publication makes use of data products from the *Wide-field Infrared Survey Explorer*, which is a joint project of the University of California, Los Angeles, and the Jet Propulsion Laboratory/California Institute of Technology, funded by the National Aeronautics and Space Administration. This publication makes use of data products from the Two Micron All Sky Survey, which is a joint project of the University of Massachusetts and the Infrared Processing and Analysis Center/California Institute of Technology, funded by the National Aeronautics and Space Administration and the National Science Foundation. We used TOPCAT[17] (Taylor 2005) for the preparation and manipulation of the tabular data and the images.

ORCID iDs

Raffaele D'Abrusco https://orcid.org/0000-0003-3073-0605
Nuria Álvarez Crespo https://orcid.org/0000-0001-5099-7169
Francesco Massaro https://orcid.org/0000-0002-1704-9850

[17] http://www.star.bris.ac.uk/~mbt/topcat/

Riccardo Campana https://orcid.org/0000-0002-4794-5453
Vahram Chavushyan https://orcid.org/0000-0002-2558-0967
Marco Landoni https://orcid.org/0000-0003-2204-8112
Fabio La Franca https://orcid.org/0000-0002-1239-2721
Nicola Masetti https://orcid.org/0000-0001-9487-7740
Dan Milisavljevic https://orcid.org/0000-0002-0763-3885
Alessandro Paggi https://orcid.org/0000-0002-5646-2410
Federica Ricci https://orcid.org/0000-0001-5742-5980

References

Abdo, A. A., Ackermann, M., Agudo, I., et al. 2010, ApJ, 716, 30
Acero, F., Ackermann, M., Ajello, M., et al. 2015, ApJS, 218, 23
Acero, F., Donato, D., Ojha, R., et al. 2013, ApJ, 779, 133
Ackermann, M., Ajello, M., Atwood, W. B., et al. 2015, ApJ, 810, 14
Ackermann, M., Ajello, M., Atwood, W. B., et al. 2016, ApJS, 222, 5
Agudo, I., Thum, C., Gómez, J. L., et al. 2014, A&A, 566, A59
Ajello, M., Atwood, W. B., Baldini, L., et al. 2017a, ApJS, 232, 18
Ajello, M., Romani, R. W., Gasparrini, D., et al. 2014, ApJ, 780, 73
Álvarez Crespo, N., Masetti, N., Ricci, F., et al. 2016b, AJ, 151, 32
Álvarez Crespo, N., Massaro, F., D'Abrusco, R., et al. 2016a, Ap&SS, 361, 316
Álvarez Crespo, N., Massaro, F., Milisavljevic, D., et al. 2016c, AJ, 151, 95
Angelakis, E., Hovatta, T., Blinov, D., et al. 2016, MNRAS, 463, 3365
Arsioli, B., Fraga, B., Giommi, P., et al. 2015, A&A, 579, A34
Berlin, A., Hooper, D., & McDermott, S. D. 2014, PhRvD, 89, 115022
Bernieri, E., Campana, R., Massaro, E., et al. 2013, A&A, 551, L5
Best, P. N., Kauffmann, G., Heckman, T. M., et al. 2005, MNRAS, 362, 9
Blandford, R. D., & Rees, M. J. 1978, BL Lac Objects, 328
Bonzini, M., Padovani, P., Mainieri, V., et al. 2013, MNRAS, 436, 3759
Böttcher, M. 2007, Ap&SS, 309, 95
Böttcher, M. 2012, in Relativistic Jets from Active Galactic Nuclei, ed. H. Krawczynski, M. Böttcher, & D. E. Harris (New York: Wiley), 17
Bruni, G., Panessa, F., Ghisellini, G., et al. 2018, ApJL, 854, L23
Campana, R., Maselli, A., Bernieri, E., et al. 2017, MNRAS, 465, 2784
Campana, R., Massaro, E., Bernieri, E., et al. 2015, Ap&SS, 360, 65
Campana, R., Massaro, E., & Bernieri, E. 2016, Ap&SS, 361, 185
Chang, Y.-L., Arsioli, B., Giommi, P., et al. 2017, A&A, 598, A17
Condon, J. J., Cotton, W. D., Greisen, E. W., et al. 1998, AJ, 115, 1693
Cowperthwaite, P. S., Massaro, F., D'Abrusco, R., et al. 2013, AJ, 146, 110
D'Abrusco, R., Massaro, F., Ajello, M., et al. 2012, ApJ, 748, 68
D'Abrusco, R., Massaro, F., Paggi, A., et al. 2013, ApJS, 206, 12
D'Abrusco, R., Massaro, F., Paggi, A., et al. 2014, ApJS, 215, 14
Dermer, C. D., & Schlickeiser, R. 1993, ApJ, 416, 458
Donoso, E., Best, P. N., & Kauffmann, G. 2009, MNRAS, 392, 617
Falomo, R., Pian, E., & Treves, A. 2014, A&ARv, 22, 73
Giroletti, M., Massaro, F., D'Abrusco, R., et al. 2016, A&A, 588, A141
Gunn, J. E., Carr, M., Rockosi, C., et al. 1998, AJ, 116, 3040
Healey, S. E., Romani, R. W., Taylor, G. B., et al. 2007, ApJS, 171, 61
Helfand, D. J., White, R. L., & Becker, R. H. 2015, ApJ, 801, 26
Helou, G., Soifer, B. T., & Rowan-Robinson, M. 1985, ApJL, 298, L7
Homan, D. C., Ojha, R., Wardle, J. F. C., et al. 2002, ApJ, 568, 99
Hovatta, T., Lindfors, E., Blinov, D., et al. 2016, A&A, 596, A78
IceCube Collaboration, Aartsen, M. G., Ackermann, M., et al. 2018, Sci, 361, eaat1378
La Mura, G., Chiaro, G., Ciroi, S., et al. 2015, JApA, 36, 447
Landoni, M., Massaro, F., Paggi, A., et al. 2015, AJ, 149, 163
Landoni, M., Paiano, S., Falomo, R., et al. 2018, ApJ, 861, 130
Lister, M. L., Aller, H. D., Aller, M. F., et al. 2009, AJ, 137, 3718
Lister, M. L., & Homan, D. C. 2005, AJ, 130, 1389
Mainzer, A., Grav, T., Bauer, J., et al. 2011, ApJ, 743, 156
Marchesi, S., Kaur, A., & Ajello, M. 2018, AJ, 156, 212
Marchesini, E. J., Peña-Herazo, H. A., Álvarez Crespo, N., et al. 2019, Ap&SS, 364, 5
Maselli, A., Massaro, F., D'Abrusco, R., et al. 2015, Ap&SS, 357, 141
Massaro, E., Giommi, P., Leto, C., et al. 2009, A&A, 495, 691
Massaro, E., Maselli, A., Leto, C., et al. 2015, Ap&SS, 357, 75
Massaro, F., Álvarez Crespo, N., D'Abrusco, R., et al. 2016, Ap&SS, 361, 337
Massaro, F., & D'Abrusco, R. 2016, ApJ, 827, 67
Massaro, F., D'Abrusco, R., Ajello, M., et al. 2011, ApJL, 740, L48
Massaro, F., D'Abrusco, R., Landoni, M., et al. 2015, ApJS, 217, 2
Massaro, F., D'Abrusco, R., Paggi, A., et al. 2013a, ApJS, 206, 13
Massaro, F., D'Abrusco, R., Paggi, A., et al. 2013b, ApJS, 209, 10
Massaro, F., D'Abrusco, R., Tosti, G., et al. 2012a, ApJ, 752, 61
Massaro, F., D'Abrusco, R., Tosti, G., et al. 2012b, ApJ, 750, 138
Massaro, F., Giommi, P., Tosti, G., et al. 2008a, A&A, 489, 1047
Massaro, F., Giroletti, M., Paggi, A., et al. 2013c, ApJS, 208, 15
Massaro, F., D'Abrusco, R., Giroletti, M., et al. 2013d, ApJS, 207, 4
Massaro, F., Landoni, M., D'Abrusco, R., et al. 2015, A&A, 575, A124
Massaro, F., Marchesini, E. J., D'Abrusco, R., et al. 2017, ApJ, 834, 113
Massaro, F., Masetti, N., D'Abrusco, R., et al. 2014, AJ, 148, 66
Massaro, F., Paggi, A., Errando, M., et al. 2013e, ApJS, 207, 16
Massaro, F., Thompson, D. J., & Ferrara, E. C. 2015, A&ARv, 24, 2
Massaro, F., Tramacere, A., Cavaliere, A., et al. 2008b, A&A, 478, 395
Mauch, T., Murphy, T., Buttery, H. J., et al. 2003, MNRAS, 342, 1117
Mücke, A., & Protheroe, R. J. 2001, APh, 15, 121
Murase, K., Dermer, C. D., Takami, H., et al. 2012, ApJ, 749, 63
Nolan, P. L., Abdo, A. A., Ackermann, M., et al. 2012, ApJS, 199, 31
Nori, M., Giroletti, M., Massaro, F., et al. 2014, ApJS, 212, 3
Orienti, M., D'Ammando, F., Giroletti, M., et al. 2014, MNRAS, 444, 3040
Padovani, P., & Giommi, P. 1996, MNRAS, 279, 526
Padovani, P., Miller, N., Kellermann, K. I., et al. 2011, ApJ, 740, 20
Paggi, A., Massaro, F., D'Abrusco, R., et al. 2013, ApJS, 209, 9
Paggi, A., Milisavljevic, D., Masetti, N., et al. 2014, AJ, 147, 112
Paiano, S., Falomo, R., Franceschini, A., et al. 2017a, ApJ, 851, 135
Paiano, S., Falomo, R., Treves, A., et al. 2019, ApJ, 871, 162
Paiano, S., Landoni, M., Falomo, R., et al. 2017b, ApJ, 844, 120
Pavlidou, V., Angelakis, E., Myserlis, I., et al. 2014, MNRAS, 442, 1693
Peña-Herazo, H. A., Marchesini, E. J., Álvarez Crespo, N., et al. 2017, Ap&SS, 362, 228
Ricci, F., Massaro, F., Landoni, M., et al. 2015, AJ, 149, 160
Schinzel, F. K., Petrov, L., Taylor, G. B., et al. 2015, ApJS, 217, 4
Stern, D., Assef, R. J., Benford, D. J., et al. 2012, ApJ, 753, 30
Stern, D., Eisenhardt, P., Gorjian, V., et al. 2005, ApJ, 631, 163
Stickel, M., Padovani, P., Urry, C. M., et al. 1991, ApJ, 374, 431
Taylor, M. B. 2005, in ASP Conf. Ser. 347, Astronomical Data Analysis Software and Systems XIV, ed. P. Shopbell, M. Britton, & R. Ebert (San Francisco, CA: ASP), 29
Urry, C. M., & Padovani, P. 1995, PASP, 107, 803
Vermeulen, R. C., & Cohen, M. H. 1994, ApJ, 430, 467
White, R. L., Becker, R. H., Helfand, D. J., et al. 1997, ApJ, 475, 479
Wright, E. L., Eisenhardt, P. R. M., Mainzer, A. K., et al. 2010, AJ, 140, 1868
Zechlin, H.-S., & Horns, D. 2012, JCAP, 11, 50